

Spontaneous emergence of two-dimensional quasibreathers in a nonlinear Schrödinger equation with nonlocal derivatives

Alexander Hrabski  and Yulin Pan **Department of Naval Architecture and Marine Engineering, University of Michigan, Ann Arbor, Michigan 48109, USA* (Received 15 September 2022; revised 25 April 2023; accepted 20 October 2023; published 14 November 2023)

We consider the nonlinear Schrödinger equation with nonlocal derivatives in a two-dimensional periodic domain. For certain orders of derivatives, we find a type of quasi-breather solution dominating the field evolution at low nonlinearity levels. With the increase of nonlinearity, the structures break down, giving way to Rayleigh-Jeans (or wave turbulence) spectra. Phase-space trajectories associated with the quasibreather solutions are found to be close to that of the linear system and almost periodic. We employ two methods to search for nearby periodic solutions (e.g., exact breathers), yet none are found. Given these distinguishing behaviors, we interpret this structure in the context of Kolmogorov-Arnold-Moser (KAM) theory.

DOI: [10.1103/PhysRevE.108.054215](https://doi.org/10.1103/PhysRevE.108.054215)

I. INTRODUCTION

Breathers are a class of features that arise in nonlinear dynamical systems that describe solutions with strong spatial localization and periodic oscillations in time. Together with solitons, breathers are considered as prototypes for rogue waves that can occur across many fields, such as water waves [1,2], optics [3], and plasma physics [4]. In mathematics, breathers are often defined as fundamental (integrable) solutions to both continuous field equations and discrete lattice problems. Breather solutions to continuous systems have been found primarily in one-dimensional (1D) nonlinear partial differential equations (PDEs), including the sine-Gordon equation [5], the nonlinear Schrödinger equation (NLS) [1–4,6], and forms of the Korteweg–De Vries (KdV) equation [7,8]. Discrete breathers [9] have been constructed as solutions to a wide variety of discrete systems, including Josephson junctions [10,11] and the Fermi-Pasta-Ulam-Tsingou (FPUT) problem [12].

Another important category of studies concerns the spontaneous emergence of coherent structures (and in particular, breathers) under the free evolution of a system. These coherent structures include discrete breathers in the FPUT problem [13] and the discrete nonlinear Schrödinger equation [14,15]. In more physical contexts (such as spontaneous emergence), coherent structures are frequently observed that exhibit *breatherlike* behavior, yet somehow do not adhere to the strict mathematical conditions on localization and periodicity that are required of breathers [16,17]. Such structures are often referred to under the looser terminology of “quasibreather.” For example, quasibreathers exist in the 1D Majda-McLaughlin-Tabak (MMT) model [18], and they are among many of the coherent structures created by the system [19–22]. As in the case of constructing exact breather solutions to PDEs, studies on spontaneous emergence are pre-

dominantly performed in 1D situations. The only exception, to our knowledge, is Ref. [23], which identifies a (quasi)breather solution to the NLS with a potential on a two-dimensional (2D) domain, but the mechanism associated with the structure remains unexplained. To date, very little is known about 2D breathers and quasibreathers in continuous systems.

In this work, we demonstrate the existence of quasibreather solutions to a family of (nonlocal) derivative NLS without a potential, realized in a 2D domain with periodic boundary conditions. In addition to being a novel 2D quasibreather in a continuous field, other remarkable and distinguishing features of the structure include (i) the quasibreather spontaneously emerges from a stochastic wave field after long-time evolution; and (ii) the quasibreather appears equivalently for both the focusing and defocusing cases, but it exists only in the weak nonlinearity regime. As the nonlinearity of the system increases, we find a breakdown of the quasibreather state with the field relaxing to the Rayleigh-Jeans spectrum. Phase-space analysis reveals almost-periodicity, motivating a numerical search for exact breather solutions that underlie the quasibreather. We employ adaptations of an existing fixed-point method as well as a recent variational method, however we find no nearby breather solutions. Given these findings, we then suggest that the state trajectory of the quasibreather is associated with a Kolmogorov-Arnold-Moser (KAM) torus, which is a distorted trajectory of the linear (integrable) system that survives when the nonlinearity is sufficiently small [24].

II. SETUP OF NUMERICAL EXPERIMENTS

The Majda-McLaughlin-Tabak (MMT) model is a family of nonlinear dispersive wave equations that have been widely used to study wave turbulence [19,25,26] and coherent structures [18–22], due to its effectiveness in representing nonlinear waves in different physical contexts. In the present work, we consider the MMT model in two spatial dimensions,

*yulinpan@umich.edu

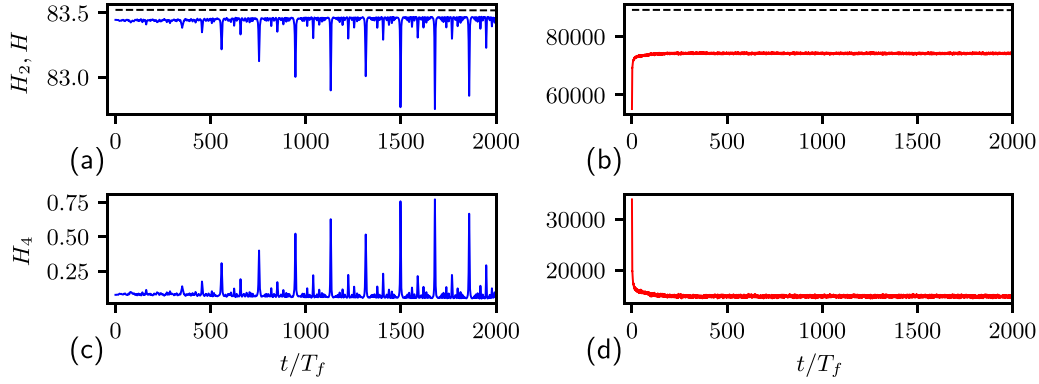


FIG. 1. The time series of H (dashed) and H_2 (solid) for (a) $\varepsilon = 0.00071$ and (b) $\varepsilon = 0.20$, as well as the corresponding H_4 for (c) $\varepsilon = 0.00071$ and (d) $\varepsilon = 0.20$. Note that a low sampling frequency is used to plot the figure to improve its readability, leading to aliasing. Therefore, only a small portion of all $O(1600)$ peaks are visible.

constructed as

$$i \frac{\partial \psi}{\partial t} = |\partial_x|^2 \psi + \lambda |\partial_x|^{\beta/4} (|\partial_x|^{\beta/4} \psi)^2 |\partial_x|^{\beta/4} \psi, \quad (1)$$

where $\psi \equiv \psi(\mathbf{x}, t)$ is a complex scalar, \mathbf{x} is the spatial coordinates, and t is the time. The nonlocal derivative operator $|\partial_x|^\alpha$ denotes a multiplication by k^α on each spectral component in the wave-number domain, with $k = |\mathbf{k}|$. The free parameter β controls the order of derivatives, and $\lambda = \pm 1$ generates a defocusing or focusing nonlinearity, respectively. Equation (1) is equivalent to a nonlocal derivative NLS, which can be shown more explicitly after a transformation $\phi = |\partial_x|^{\beta/4} \psi$, leading to

$$i \frac{\partial \phi}{\partial t} = |\partial_x|^2 \phi + \lambda |\partial_x|^{\beta/2} (|\phi|^2 \phi). \quad (2)$$

The MMT model (1) can be derived from a Hamiltonian $H = H_2 + H_4$, with

$$\begin{aligned} H_2 &= \int \|\partial_x \psi\|^2 dx, \\ H_4 &= \frac{1}{2} \lambda \int \|\partial_x^{|\beta/4} \psi\|^4 dx. \end{aligned} \quad (3)$$

The nonlinearity level of the system can be quantified via a parameter $\varepsilon \equiv H_4/H_2$.

We solve (1) on a 2D domain with periodic boundary conditions, starting from an initial field $\psi_0 \equiv \psi(\mathbf{x}, t = 0)$, via a pseudospectral method [26–28] with 128×128 modes. Our numerical method treats the linear term via an integrating factor, and the nonlinear term via an explicit fourth-order Runge-Kutta scheme. The initial field ψ_0 is set as an exponential form in Fourier space as $\hat{\psi}_0(\mathbf{k}) = A \exp[-0.1|k - k_p| + i\theta_k]$, where $k_p = 4$, and θ_k is a random phase that is decorrelated for all \mathbf{k} . Such an initial condition represents a “typical” setup for the study of out-of-equilibrium dynamics in the MMT system, where the spread of energy from k_p is generally of interest. In Appendix A, we demonstrate the existence of the breather for a higher-resolution field with different k_p , with completely different random phase realizations. In this sense, the emergence of the quasibreather does not rely on initial conditions with a specific phase coherence, but rather emerges from a random field. To investigate dynamics at dif-

ferent nonlinearity levels, we choose a range of A leading to approximately $\varepsilon \in [0.0005, 0.1]$ for each β value of interest.

III. RESULTS

We start by describing a typical simulation leading to a quasibreather state, with parameters $\beta = 3$ and $A = 35$ (corresponding to $\varepsilon = 0.00071$). Figures 1(a) and 1(c) show the long-time evolution of H_2 and H_4 from $t = 0$ to $2000T_f$, with $T_f = 2\pi$ the period of the fundamental wave mode. The total Hamiltonian H , as shown in Fig. 1(a), is well conserved over $2000T_f$. After an initial evolution of about $400T_f$ with smooth profiles of H_2 and H_4 , we observe that H_4 undergoes strong periodic jumps with corresponding dips in H_2 . These jumps are associated with coherent structures, which are only present at low nonlinearity. In contrast, as demonstrated in Figs. 1(b) and 1(d), the field evolution at a higher nonlinearity ($\varepsilon = 0.20$) exhibits smooth profiles of H_2 and H_4 over the same time interval.

The oscillations in H_4 correspond to oscillations of a quasibreather. To better visualize this state, we plot in Fig. 2 the real part of ψ at different phases of its oscillations (i.e., different stages of the oscillation pattern in H_4). Figure 2(a) shows the field right before the first jump of H_4 , where a concentric wave appears and later converges into a peak seen in Fig. 2(b). This peak then collapses, with a second one emerging after about $T_f/2$ [according to Fig. 2(e)] at the maximally distant location in the periodic domain, shown in Fig. 2(c). The cycle then repeats itself with a peak emerging in Fig. 2(d) [at the same location as in Fig. 2(a)], forming a quasibreather solution coexisting with a stochastic wave background. The smaller peaks of H_4 seen in Fig. 2(e) correspond to groups of secondary peaks in ψ , as shown in Figs. 3(a)–3(d). To better resolve the smaller amplitudes of these secondary structures, we choose to plot $|\psi|$ rather than $\text{Re}[\psi]$. We encourage the reader to also watch the animation of the full quasibreather cycle in the Supplemental Material [29]. From Fig. 2 we see that the quasibreather oscillates with a fundamental period very close to T_f . Therefore, the simulation in Figs. 1(a) and 1(c) covers $O(1600)$ cycles of the breather, demonstrating a very long (perhaps infinite) time of existence.

We next investigate the existence and intensity of the quasibreaters for varying values of β and ε . To measure

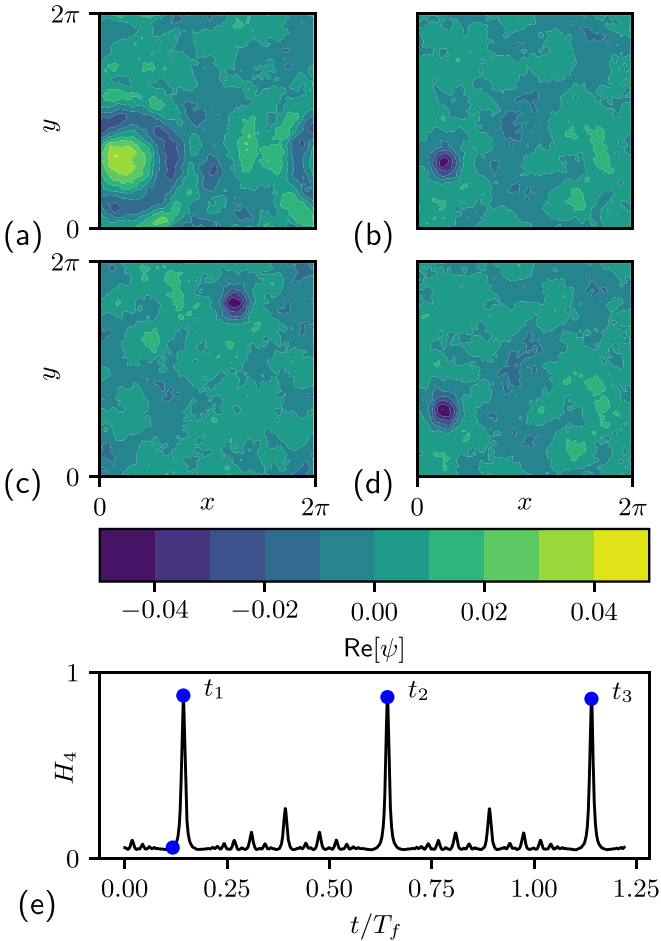


FIG. 2. Contour plots of $\text{Re}[\psi]$ at $\beta = 3$ for $\varepsilon = 0.000\,71$ at various stages of the cycle of the quasibreather (a)–(d), corresponding chronologically to the times marked by the blue circles in (e) the time series of H_4 . Note that this plot of H_4 has sufficient sampling to resolve all features.

the relative intensity of the peak, we define the peak-to-background ratio as

$$\rho = \frac{\text{avgmax}[|\psi|]}{4\sigma_{|\psi|}}, \quad (4)$$

where the avgmax operator returns the average of the maximum height of primary peaks [as in Figs. 2(b)–2(d)] over many cycles of the quasibreather, and $\sigma_{|\psi|}$ is the total standard deviation of the field $|\psi|$ over space and time. By definition (4), $\rho = 2$ corresponds to the typical rogue wave criterion used in many fields [3].

Figure 4(a) shows the value of ρ obtained for $\beta = 0, 1, 2, 3, 4$ and ε across three orders of magnitude. In general, we see that the quasibreather state is present for smaller ε (i.e., weak nonlinearity) and becomes stronger when β is closer to 3. The case with $\beta = 0$ (corresponding to NLS) leads to no quasibreathers, indicating the derivative is necessary for their emergence. We note that when the breathers are not present, the value of ρ is evaluated by taking the average of the maximum of the field $|\psi|$ every $T_f/2$ as the numerator in (4). The physical role of β in determining the existence and

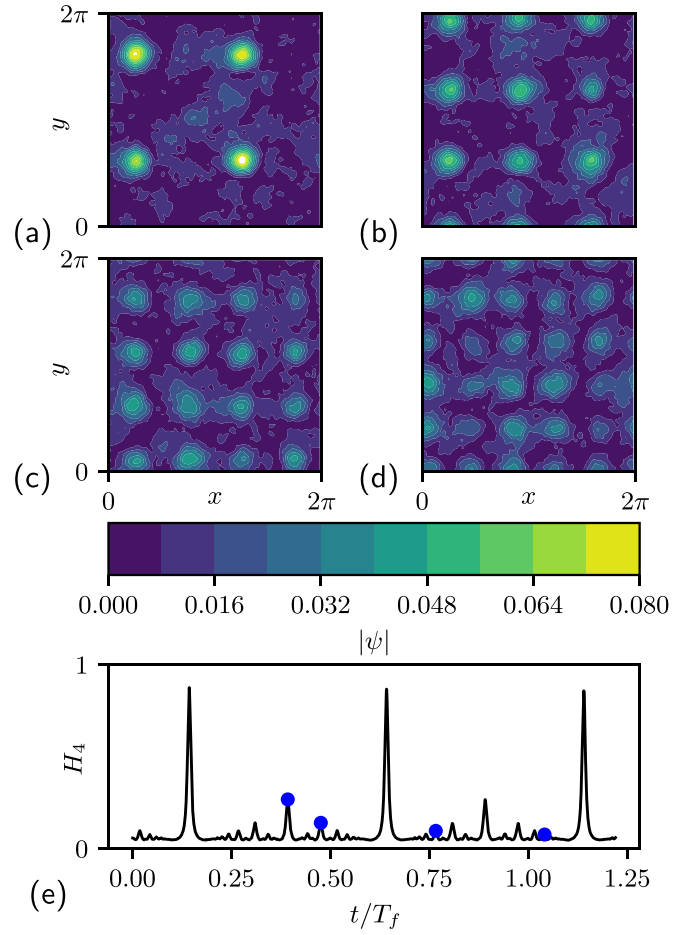


FIG. 3. Contour plots of $|\psi|$ at $\beta = 3$ for $\varepsilon = 0.000\,71$ detailing secondary structures in the quasibreather (a)–(d) cycle, corresponding chronologically to the times marked by the blue circles in (e) the time series of H_4 .

intensity of this structure clearly needs further study, which will not be covered in this paper.

Furthermore, we examine in Fig. 4(b) the slope γ of the stationary wave action spectrum $n(\mathbf{k}) \equiv \langle \hat{\psi}(\mathbf{k})\hat{\psi}^*(\mathbf{k}) \rangle$ across all values of β and ε . The inset of Fig. 4(b) shows a typical example of fully developed, angle-averaged $n(k)$ for $\beta = 2$ and several values of ε . We see that the Rayleigh-Jeans spectrum with $\gamma = -2$ is only achieved at higher nonlinearity when the breather is not present. This trend is generally true for all values of β as shown in Fig. 4(b).

A few additional remarks are in order. First, we note that the quasibreather also emerges for the focusing equation (1) with $\lambda = -1$ under the same conditions. Second, the quasibreather can also be observed under a forced/dissipated system [28], but with relaxation to wave turbulence spectra at high nonlinearity. Last but not least, we have performed extensive numerical analysis to verify that the breather we observe is not a numerical artifact. This includes verification of the robustness of our results under symplectic integration, higher resolution, and different dealiasing schemes. Details of all of the above points can be found in Appendixes A–C, respectively.

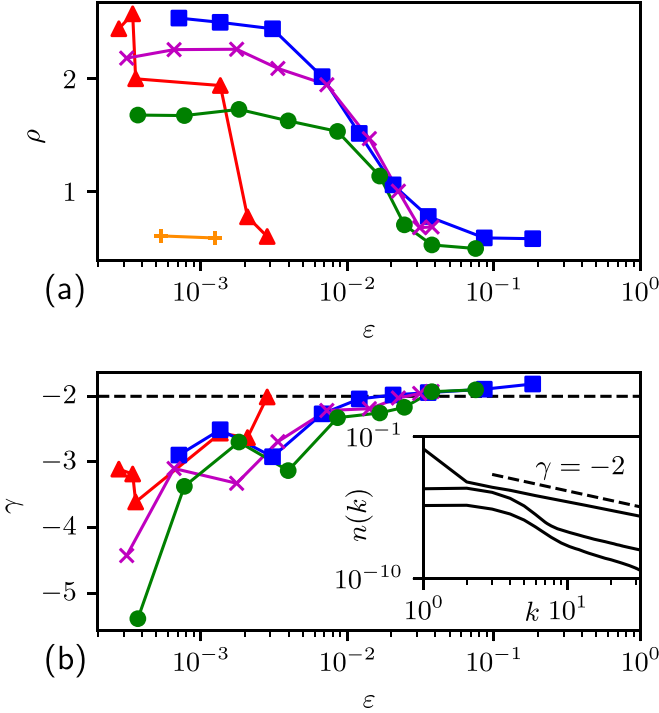


FIG. 4. The quantities (a) ρ and (b) γ as functions of ε for $\beta = 0$ (orange +), $\beta = 1$ (green ●), $\beta = 2$ (magenta ×), $\beta = 3$ (blue ■), and $\beta = 4$ (red ▲). The inset of (b) shows fully developed, angle-averaged wave action spectra at a few nonlinearity levels (for $\beta = 3$), with the Rayleigh-Jeans spectral slope of $\gamma = -2$ indicated (dashed).

IV. SEARCH FOR PERIODIC SOLUTIONS

The quasibreather solution in our simulation is close to (but not exactly) periodic, which is evident from the slightly varying field at each moment of the peak (not shown here). In fact, the almost-periodicity of the quasibreather distinguishes it from an exact breather. Because the quasibreather is close to periodic, we are interested in whether there exists a nearby trajectory that corresponds to an exactly periodic breather that supports the quasibreather dynamics. For this purpose, we have employed both a traditional spectral method [30] based in fixed-point iteration and a very recent variational method [31] for seeking nearby, exactly periodic breather solutions. We begin with the fixed-point method.

A. Spectral fixed-point method

The spectral method by Flach uses fixed-point iteration to obtain breathers in a Hamiltonian lattice. Our problem is in some sense similar, as we can interpret our problem on a lattice of Fourier modes in the wave-number domain. After assuming a periodic solution in time, we may now express the field in terms of A_{kn} , where n indicates the n th temporal harmonic of $\hat{\psi}_k$ with frequency $\Omega_n = n$, assuming a periodic solution with $T = 2\pi$. We then write a system of equations derived from (1) in terms of A_{kn} ,

$$(k^2 - \Omega_n)A_{kn} + \gamma F_{kn} = 0, \quad (5)$$

where F_{kn} is the fully spectral form of the nonlinear term in (1), and γ is a parameter we introduce to vary the size of

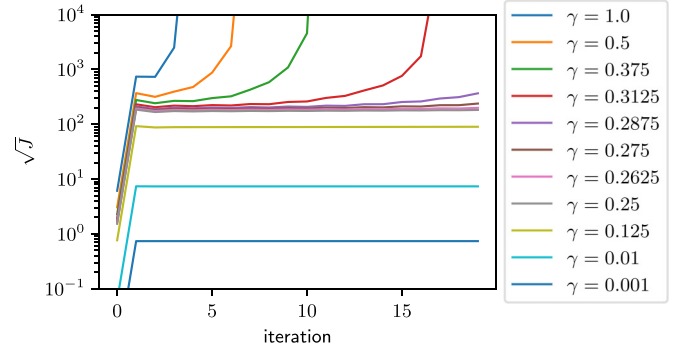


FIG. 5. The residual of (5) against iteration number for various choices of γ .

the nonlinearity. Solutions to this equation represent periodic solutions to (1). Using an adaptation of Flach’s fixed-point method, we attempt to find solutions to this equation. Details on our adaptation of Flach’s procedure can be found in Appendix C. Iteration begins with an initial condition of a full period of the quasibreather solution at nonlinearity level $\varepsilon = 0.0008$ and $\beta = 3$.

The L^2 norm of the residual $\sqrt{J} \equiv \|R\|_2$ of (5) is provided at each iteration up to $N_{\text{iter}} = 20$ for a wide variety of γ in Fig. 5. It is clear that, even for the smallest γ , the residue does not drop to zero. In fact, the residue always diverges under a finite number of iterations. Thus, our adaptation of Flach’s fixed-point iteration method [30] does not furnish the desired breather solution.

B. Variational method

Next, we implement the variational method by Azimi *et al.* [31]. The goal of their method is to numerically obtain periodic solutions to high-degree-of-freedom systems. This is done by finding a new dynamical system whose attractors are (potentially) periodic solutions to the equation of interest. This new dynamical system is defined in the space of all periodic orbits that obey the periodic boundary conditions (the “loop space”). Thus, evolution of this new dynamical system is not with respect to the physical time (which is a dimension of the loop space), but rather to a parameter τ referred to as “fictitious time.” As this system is propagated in τ , the initial loop (a guess of a periodic solution) relaxes towards true periodic solutions to the equation of interest. If a residual of zero is obtained, a periodic solution has been identified.

Before directly applying their method for obtaining such a system, however, we first must modify it to accommodate the MMT equation. These changes are significant enough to warrant a detailed discussion, provided in Appendix C. For now, it will suffice to state that their method returns the period T , the proposed periodic solution $\hat{\psi}_k$, and \sqrt{J} as the L_2 -norm residual of the MMT equation for the proposed periodic solution.

We choose as an initial condition one full cycle of the quasibreather at very low nonlinearity ($\varepsilon = 0.0004$), for which the system is very close to periodic. To reduce the stiffness of the system, we choose the $\beta = 1$ case. A snapshot of the initial condition is contained in Fig. 6(a). The system is then evolved in fictitious time. As expected, the residual norm J

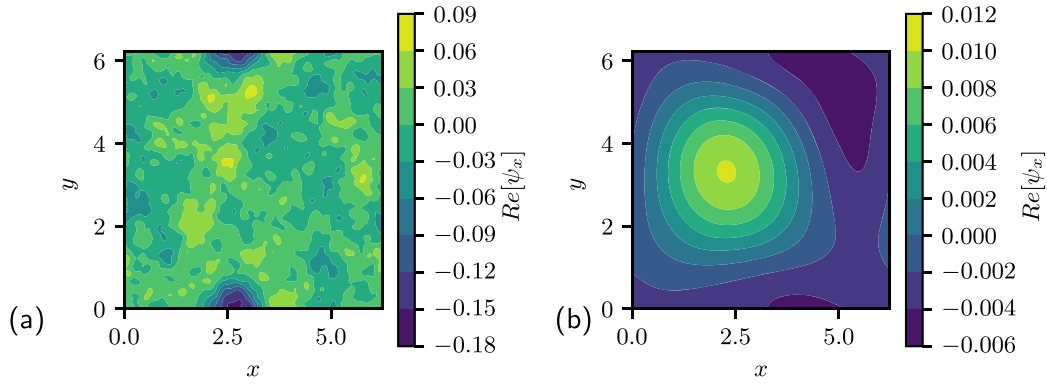


FIG. 6. (a) A snapshot of the initial condition I_0 in the variational method; (b) a snapshot of the solution at $\tau = 50$, i.e., after 5000 time steps.

decreases monotonically, as depicted in Fig. 7(a). We do not simulate long enough to reach a steady value of J , as after just $\tau = 50$ (~ 5000 time steps) we already can see that the loop has strongly diverged from the expected breather pattern. The corresponding snapshot of the initial breather peak after $\tau = 50$ is contained in Fig. 6(b). The position, shape, and magnitude of the resolved peak are all drastically different from the exactly periodic breather we seek. This is also depicted in a growth of T [Fig. 7(b)] beyond the expected $T \approx 2\pi$. From the above observations, it is clear that the variational method does not find a nearby breather solution. We also note that there may be certain modifications we can make to this method, e.g., to preserve the Hamiltonian of the solution through a Lagrangian multiplier term, which may provide a different solution. These challenges will not be tackled in the current work.

V. DISCUSSION

Although our search for an underlying periodic breather is in some sense insightful, neither of these techniques returns a periodic solution that resembles the breather we have observed. While this certainly may be due to limitations of the methods we employ, it strongly suggests a lack of periodic structures close to our near-periodic breather solution. If this is the case, the quasibreather solution may be quasiperiodic by nature and will require a new physical interpretation.

We start by stating that there exists an exact periodic solution to the linear system of (1), i.e., $H_4 = 0$, that closely resembles the quasibreather we observe. What we mean precisely is that, starting from an initial condition with a breather peak [say, Fig. 2(b)], the field propagated by the linear equation returns to the same state after exactly T_f , which is consistent with the pattern of a breather. This is because the linear system only contains integer frequencies due to the NLS dispersion relation $\omega = k^2$, so that T_f is the period of the linear system. This fact suggests that the quasibreather solution to the nonlinear system arises from a deformed trajectory of the linear system.

Since visualizing the high-dimensional trajectory is very difficult, we define a projection of the trajectory to some physically meaningful reference field [23]:

$$I_n = \left| \frac{\int \psi_R^*(\mathbf{x}, t_n) \psi(\mathbf{x}, t) d\mathbf{x}}{\int \psi_R^*(\mathbf{x}, t_n) \psi_R(\mathbf{x}, t_n) d\mathbf{x}} \right|, \quad (6)$$

where $\psi_R^*(\mathbf{x}, t_n)$ is the reference field where a quasibreather peak is present, e.g., taken from t_1 in Fig. 2(e), and $\psi(\mathbf{x}, t)$ is the solution of either the linear or nonlinear system propagated from $\psi_R^*(\mathbf{x}, t_n)$. Figure 8 shows the evolution of I_1 from both linear and nonlinear systems for a range of four nonlinearity levels. It is clear that the linear system evolution exhibits a period of T_f in all subfigures as expected. When the nonlinearity level is low, the trajectory identified by I_1 shows a small deformation from the linear trajectory, as seen in Fig. 8(a). Such deformation is consistent with a

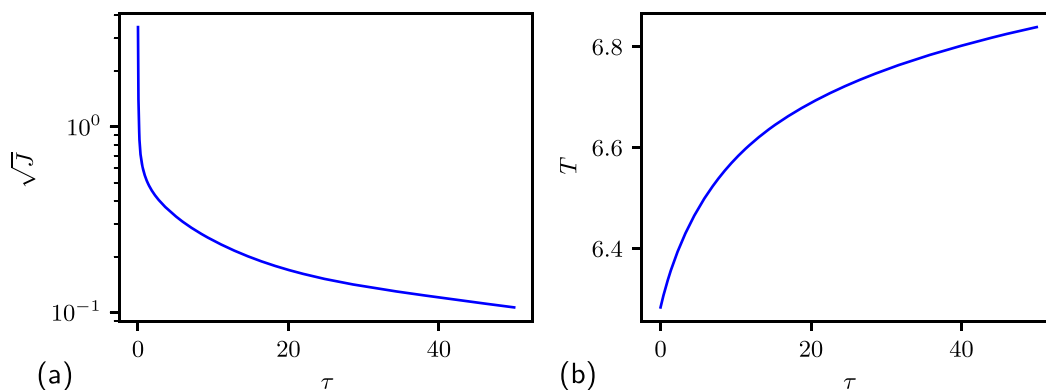


FIG. 7. The change of (a) residue norm \sqrt{J} and (b) period T as functions of τ in the variational method.

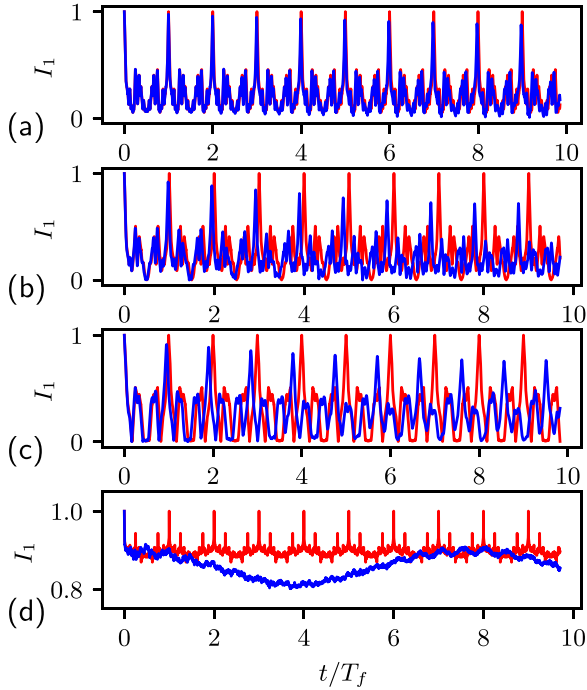


FIG. 8. I_1 evaluated for the nonlinear system $\beta = 3$ (blue) and the linear system (red) for (a) $\varepsilon = 0.00071$, (b) $\varepsilon = 0.0084$, (c) $\varepsilon = 0.013$, and (d) $\varepsilon = 0.20$.

high-dimensional quasiperiodic trajectory that is evident from not only the gradual time shift of the I_1 peak, but also the deviation of the I_1 peak from 1. As the nonlinearity level increases, we observe an increased deformation of the trajectory, until the linear trajectory is entirely destroyed at high nonlinearity in Fig. 8(d). This trajectory deformation can also be observed in the (I_1, I_2) plane in Fig. 9, as well as in animations included the Supplemental Material [29].

The trajectory deformation visualized above can be connected to Kolmogorov-Arnold-Moser (KAM) theory. Specifically, if we consider the linear system as the base integrable system, then the nonlinear term can be considered as the perturbation added to the system to form a nearly integrable system. Generally speaking, if the perturbation is sufficiently small, some quasiperiodic trajectories of the integrable system can be preserved with small deformation to a KAM torus [24]. In our case, these preserved trajectories (i.e., KAM tori) would correspond to those associated with the quasibreather solution observed in Fig. 2. We also note that the linear system of Eqs. (1) (or more generally the NLS) is resonant, which makes it difficult to directly apply the KAM theory. Most mathematical work of KAM on NLS relies on some way to introduce irrational frequencies, e.g., by including a potential term as in [32], and only a handful of results are available for application of KAM to NLS itself (see [33,34]). Our results, therefore, suggest that quasibreather solutions can be supported by KAM tori when a nonlocal derivative is included in the NLS. These quasibreather solutions break down at high nonlinearity due to the sufficiently strong perturbation to the KAM tori. The necessity of weak nonlinearity in observing these quasibreaters is also consistent with mathematical descriptions of quasiperiodic (quasi)breaters via KAM and

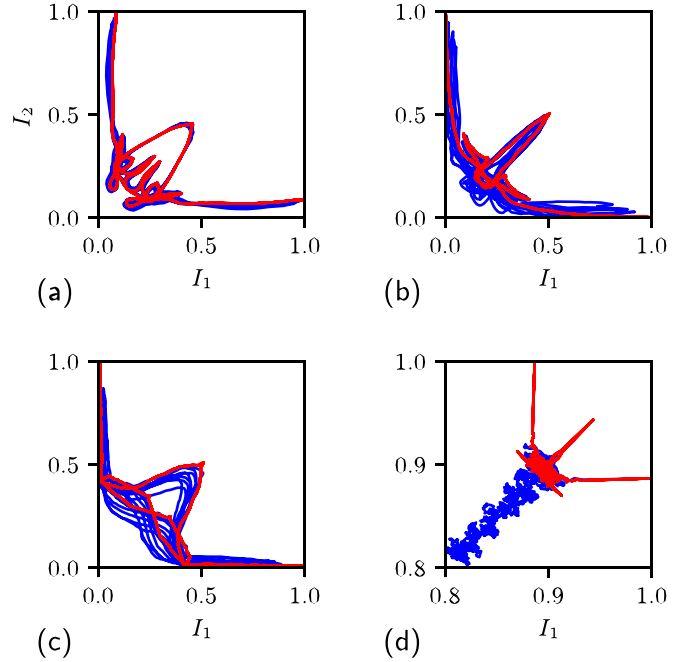


FIG. 9. The trajectory of ψ projected onto I_1 and I_2 for several fundamental periods of ψ computed via the nonlinear system $\beta = 3$ (blue) and the linear system (red) for (a) $\varepsilon = 0.00071$, (b) $\varepsilon = 0.0084$, (c) $\varepsilon = 0.013$, and (d) $\varepsilon = 0.20$.

related theorems in Hamiltonian lattices, which rely explicitly on weak lattice coupling [35–37].

Finally, the current analysis clearly does not resolve all the questions regarding the 2D quasibreather solution. One issue is that finite-time numerical simulations cannot be used as rigorous proof for the existence of KAM tori (which must exist for infinite time). Therefore, our interpretation may need to be understood in terms of the Nekhoroshev theorem, which proves the existence of nearly integrable trajectories for finite but very long times [24]. Another critical question is the stochastic emergence of these stable quasibreather solutions. One possible interpretation is that they lie on some type of statistical “attractor” [38], such that a variety of initial conditions lead to the quasibreather state. In addition, while the quasibreather we find here is for a derivative NLS not specific to a physical system, we remark that such equations are generally involved in the fields of nonlinear water waves, optics, and others. For example, the (quasi)breaters recently found both experimentally and numerically in a Bose-Einstein condensate [23] may bear a similar physical interpretation to the one we provide here. Lastly, the dependence of the breather’s existence and intensity on β is an interesting and open question. We suggest that further mathematical inquiry in the context of the KAM theorem may shed light on this issue. Specifically, we hope that a rigorous description of this structure might explain why $\beta = 0$ precludes it.

VI. CONCLUSION

In this paper, we present results regarding a quasibreather that spontaneously emerges from a 2D nonlocal derivative NLS. We show that the quasibreather emerges at low

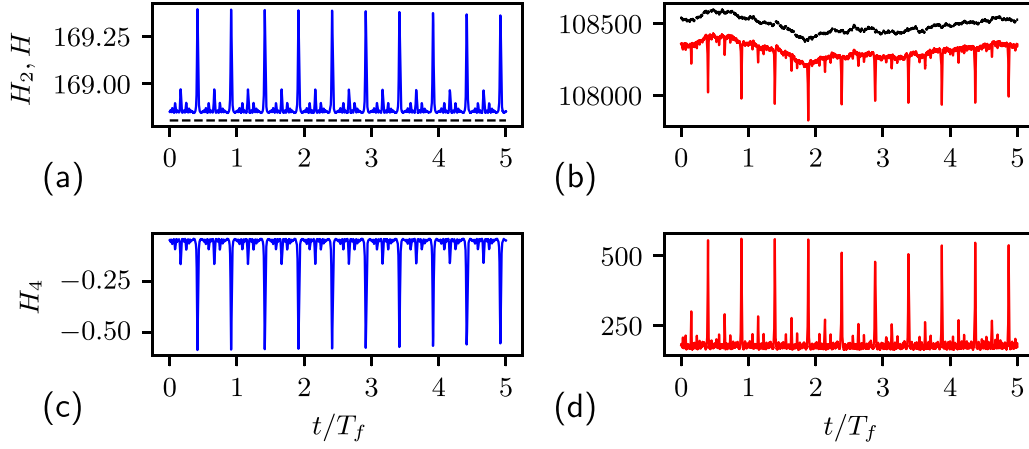


FIG. 10. $5T_f$ of the time series of H (dashed) and H_2 (solid) for a fully developed quasibreather solution to (a) the focusing MMT equation with $\beta = 3$, and (b) the forced-dissipated MMT equation with $\beta = 2$. The corresponding H_4 for (c) the focusing system and (d) the forced-dissipated system is also provided. The focusing system has $\varepsilon = 0.00028$ and the forced-dissipated system has $\varepsilon = 0.0016$.

nonlinearity with parameter β close to 3. A phase-space analysis reveals that the trajectory associated with the quasibreather solution is close to that of the linear system, but with almost-periodicity introduced by the nonlinearity. This almost-periodicity motivates a numerical search for nearby exact breather solutions, but none are found. Our results support an explanation of the quasibreather solution by KAM theory, in the sense that a solution of the linear system is deformed but preserved when a small nonlinearity is introduced.

ACKNOWLEDGMENTS

We thank Filippo Giuliani, Benno Rumpf, Bobby Wilson, Peter Miller, Zaher Hani, Gigliola Staffilani, and Ricardo Grande for their thoughtful comments and suggestions. This material is based upon work supported by the National Science Foundation Graduate Research Fellowship under Grant No. DGE 1841052. Any opinions, findings, and conclusions or recommendations expressed in this material are those of the authors and do not necessarily reflect the views of the National Science Foundation. This work used the Extreme Science and Engineering Discovery Environment (XSEDE), which is supported by National Science Foundation Grant No. ACI-1548562. Computation was performed on XSEDE Bridges-2 at the Pittsburgh Supercomputing Center through allocation PHY200041. This research was supported in part through computational resources and services provided by Advanced Research Computing (ARC), a division of Information and Technology Services (ITS) at the University of Michigan, Ann Arbor.

APPENDIX A: QUASIBREATHER SOLUTIONS IN OTHER SITUATIONS

In this Appendix, we show the occurrence of the quasibreather in additional contexts: the MMT model with a focusing nonlinearity, as well as a defocusing forced-dissipated model.

We begin with the focusing MMT model. The focusing case is given by Eqs. (1) and (2) with $\lambda = -1$. The parameter

λ is well known to control the modulational instability of the nonlinear Schrödinger equation (NLS) as well as the MMT model. In the context of the MMT model, the sign of λ has been shown to affect the emergence of coherent structures in a one-dimensional MMT model with dispersion relation $\omega = k^{1/2}$ [21]. In our results, however, we find no significant change in the quasibreather behavior between the focusing/defocusing equations, suggesting (along with the fact that the breather exists only at *weak* nonlinearity) that modulational instability is not responsible for the quasibreather. In Figs. 10(a) and 10(c), we show five fundamental periods T_f of H and its components H_2 and H_4 in a fully developed quasibreather state for the focusing equation with $\beta = 2$. These results were obtained with an identical numerical setup to the one presented in Sec. II, and they are taken at low nonlinearity. The pattern of oscillation in H_2 and H_4 is also similar to that in the defocusing case.

Next, we present results obtained for a forced-dissipated system. We again solve the defocusing 2D MMT model (with $\beta = 2$), however with the addition of forcing and dissipation terms. Specifically, we solve the equation

$$i \frac{\partial \psi}{\partial t} = |\partial_x|^2 \psi + \lambda |\partial_x|^{\beta/4} (|\partial_x|^{\beta/4} \psi)^2 |\partial_x|^{\beta/4} \psi + F + D_1 + D_2, \quad (\text{A1})$$

where F represents the forcing, and D_1 and D_2 represent dissipation. These terms are explicitly defined in a spectral domain, where

$$F = \begin{cases} F_r + iF_i, & 7 \leq k \leq 9, \\ 0 & \text{otherwise,} \end{cases} \quad (\text{A2})$$

with F_r and F_i sampled from a Gaussian distribution of zero-mean, producing a standard white-noise forcing. The dissipative terms are defined as

$$D_1 = \begin{cases} -iv_1 \hat{\psi}_k, & k \geq 100, \\ 0 & \text{otherwise,} \end{cases} \quad D_2 = \begin{cases} -iv_2 \hat{\psi}_k, & k \leq 7, \\ 0 & \text{otherwise,} \end{cases} \quad (\text{A3})$$

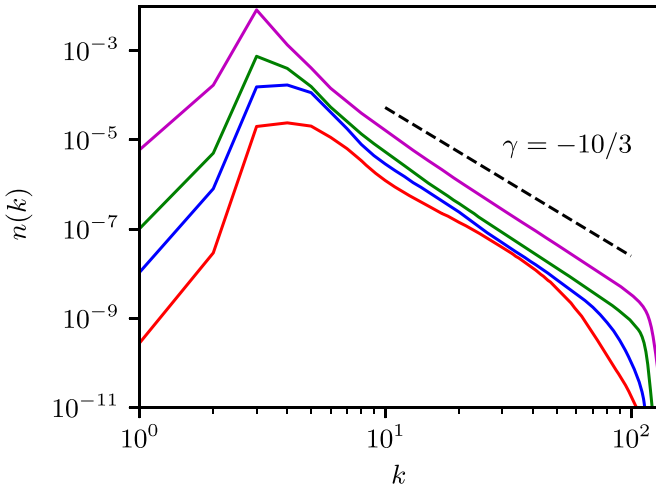


FIG. 11. The fully developed, angle-averaged wave action spectra at a few nonlinearity levels of the forced-dissipated system, with the Kolmogorov-Zakharov spectral slope of $\gamma = -10/3$ indicated (dashed).

where ν_1 and ν_2 are dissipative constants. We solve these equations on a larger domain of 512×512 modes for nearly identical initial conditions, with the initial spectral peak now at $k_p = 10$. In Fig. 10(b), H and its two components are plotted for $5T_f$ in the quasibreather state. In this case, we do not expect the total Hamiltonian to be conserved, but rather to be quasisteady for the fully developed system. Nevertheless, the signature of the quasibreather is clearly present. Just as in the unforced case, we find that the wave action spectrum of the system is altered by the quasibreather. In Fig. 11, we provide the fully developed spectra of the forced-dissipated system for several different orders of nonlinearity. When the nonlinearity is low and the quasibreather is present, we again see a departure from a power-law spectrum, with a steeper tail region. When nonlinearity is raised, we observe that the spectra of wave turbulence are restored (and an associated forward energy cascade develops) [28].

APPENDIX B: NUMERICAL VALIDATION OF THE QUASIBREATHER

In this Appendix, we provide analyses and numerical tests that rule out the possibility that the structure we discuss is a numerical artifact. In particular, we show that the quasibreather solution is consistent under the following:

- (i) The change of integration scheme to a symplectic integrator.
- (ii) The change of our dealiasing procedure.
- (iii) An increase in the number of Fourier modes (spatial resolution).

We begin with point (i). Symplectic integration of a Hamiltonian system preserves the phase-space geometry of its solution. Specifically, under Hamiltonian flow, structures such as sinks and limit cycles are forbidden by Liouville's theorem. When using an integrator such as an explicit fourth-order Runge-Kutta scheme (RK4), however, these structures can be erroneously introduced into the solution, which may change the dynamics. To ensure the quasibreather is not an artifact introduced by nonsymplectic integration, we implement a simple symplectic integrator, the implicit midpoint method (IMP) [39], to verify that we still obtain (and preserve) the quasibreather solution. In the IMP method, we solve the implicit nonlinear problem via fixed-point iteration. For an identical numerical setup to that of the main paper, we allow the system to freely evolve under the IMP integration scheme. We set $\beta = 3$ and simulate at the low nonlinearity of $\varepsilon = 0.001$.

We provide in Fig. 12(a) the evolution of H and H_2 from $t = 0$, with H very well conserved and H_2 indicating that the quasibreather has already formed by $t = 1000T_f$. The corresponding plot of H_4 is provided in Fig. 12(c). Just as in Fig. 1, these plots of the initial evolution have a low sampling rate, leading to aliasing. To confirm that the quasibreather has the same signature in H_2 and H_4 as in the case of nonsymplectic integration, high-sampling rate plots of H , H_2 [Fig. 12(b)] and H_4 [Fig. 12(d)] are also provided over $5T_f$, showing no difference from the results presented in the main text. Thus, the quasibreather is not an artifact of nonsymplectic integration.

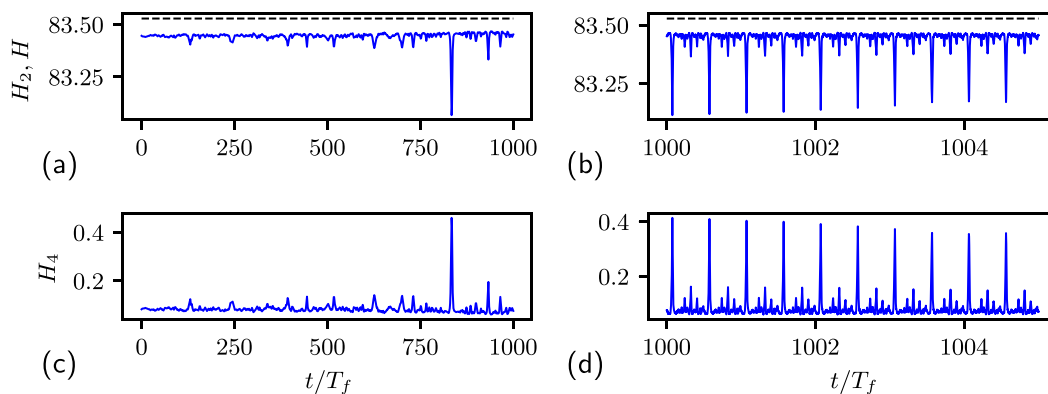


FIG. 12. The time series of (a) H (dashed) and H_2 (solid) starting from $t = 0$ for the defocusing MMT equation with $\beta = 3$ under symplectic integration, with the corresponding time series of (c) H_4 . A detailed view beginning at $t = 1000T_f$ of (b) H , H_2 and (d) H_4 over $5T_f$.

Next, we address point (ii). To prevent the aliasing of modes due to the cubic nonlinearity of the MMT model, a standard 1/2 dealiasing rule is applied after each product during the evaluation of the nonlinear term. The 1/2 dealiasing rule is typically implemented via zero-padding the truncated wave-number domain: if k_m is the maximum resolved wave number in our simulation (that is oriented along the x and y axes), then, in each direction, zero-padding is included such that for a computation domain of size $[-2k_m, 2k_m]^2$, the nonzero (resolved) Fourier modes are only contained in the box $[-k_m, k_m]^2$. The zero-padding is enforced by setting all

modes outside the box $[-k_m, k_m]^2$ to zero after each product is taken.

This procedure, however, has the effect of subtly changing the evolution of the system. To be assured that the quasibreather is not an artifact of our dealiasing scheme, we first show that our dealiasing leads to a slightly modified Hamiltonian system (analytically), and then we show that the quasibreather is preserved in the original system without modification. We start by writing down the truncated Hamiltonian that we aim to numerically simulate:

$$H = \sum_{|\mathbf{k}|_\infty \in [-k_m, k_m]} k^2 \hat{\psi}_{\mathbf{k}} \hat{\psi}_{\mathbf{k}}^* + \frac{1}{2} \lambda \sum_{\substack{k_1, k_2, k_3, k \\ k_1 + k_2 = k_3 + k \\ |\mathbf{k}_i|_\infty \in [-k_m, k_m]}} (k_1 k_2 k_3 k_4)^{\beta/4} \hat{\psi}_{\mathbf{k}_1} \hat{\psi}_{\mathbf{k}_2} \hat{\psi}_{\mathbf{k}_3}^* \hat{\psi}_{\mathbf{k}}^*, \quad (\text{B1})$$

where the summation is over every permutation over the subscript wave numbers. When computing the nonlinear term, we evaluate (via the Fourier transform)

$$(\psi_x \psi_x^*) \psi_x = \left(\sum_{\substack{k_1, k_3 \\ |\mathbf{k}_i|_\infty \in [-k_m, k_m] \\ |\mathbf{k}_1 - \mathbf{k}_3|_\infty \in [-k_m, k_m]}} \hat{\psi}_{\mathbf{k}_1} \hat{\psi}_{\mathbf{k}_3}^* e^{i(\mathbf{k}_1 - \mathbf{k}_3) \cdot \mathbf{x}} \right) \sum_{|\mathbf{k}_2|_\infty \in [-k_m, k_m]} \hat{\psi}_{\mathbf{k}_2} e^{i\mathbf{k}_2 \cdot \mathbf{x}}, \quad (\text{B2})$$

where the derivatives have been neglected for clarity ($\beta = 0$). The second condition under the first sum (red) is the first dealiasing step, where any product of modes that is mapped outside the bounded computational domain is excluded from the sum. The effect of dealiasing is therefore to remove certain interactions from the original system. It is not hard to show that including this extra condition modifies the Hamiltonian such that

$$H' = \sum_{|\mathbf{k}|_\infty \in [-k_m, k_m]} k^2 \hat{\psi}_{\mathbf{k}} \hat{\psi}_{\mathbf{k}}^* + \frac{1}{2} \lambda \sum_{\substack{k_1, k_2, k_3, k \\ k_1 + k_2 = k_3 + k \\ |\mathbf{k}_i|_\infty \in [-k_m, k_m] \\ |\mathbf{k}_1 - \mathbf{k}_3|_\infty \in [-k_m, k_m]}} (k_1 k_2 k_3 k_4)^{\beta/4} \hat{\psi}_{\mathbf{k}_1} \hat{\psi}_{\mathbf{k}_2} \hat{\psi}_{\mathbf{k}_3}^* \hat{\psi}_{\mathbf{k}}^*, \quad (\text{B3})$$

where H' represents the effective Hamiltonian when dealiasing is used. While a second dealiasing step is included after the second product is taken in (B2), no additional interactions are removed from H' by the second dealiasing step: $|\mathbf{k}_1 + \mathbf{k}_2 - \mathbf{k}_3|_\infty \in [-k_m, k_m]$ is accounted for by the fact that we already require $\mathbf{k}_1 + \mathbf{k}_2 - \mathbf{k}_3 = \mathbf{k}$ and $|\mathbf{k}|_\infty \in [-k_m, k_m]$. We remark that it is not *a priori* clear that the dealiasied system is still a Hamiltonian, but this fact is discovered when one attempts to write H' .

To show that the system evolution according to (B1) also leads to the quasibreather solution, we perform a different dealiasing scheme for the simulation. Specifically, we skip the dealiasing step in the intermediate stage of computing the cubic term, and only dealias once after cubic multiplication is completed. Since this dealiasing step is equivalent to keeping only the Fourier modes up to k_m , this strategy produces evolution consistent with the system given by H (rather than H'). We use this scheme in an otherwise identical setup to the main text, with $\beta = 3$ and $\varepsilon = 0.001$, simulating until a quasibreather emerges.

The evolution of the Hamiltonian H and the component H_2 from $t = 0$ are presented in Fig. 13(a), and the corresponding H_4 is in Fig. 13(c). For this supplemental test, we use a larger

time step that leads to larger dissipation, though the energy loss over $1000T_f$ it is still only 0.5% of the total energy. We see that a clear peak in H_4 has formed before $t = 1000T_f$, indicating the quasibreather has formed. Again, due to the low sampling rate, aliasing is present in Figs. 13(a) and 13(c). We provide detailed plots over $5T_f$ of H, H_2 in Fig. 13(b) and H_4 in Fig. 13(d) with sufficient sampling such that no aliasing is present. It is clear that the quasibreather remains unchanged under our second scheme, which preserves the truncated Hamiltonian system, indicating that the structure is not an artifact of dealiasing.

Finally, we address point (iii). The forced-dissipated results shown in Sec. I are computed on a domain with 16 times as many modes, which shows that the quasibreather emerges and persists in simulations with higher spatial resolution.

APPENDIX C: SEARCH FOR NEARBY PERIODIC SOLUTIONS

In this Appendix, we detail the methods we have implemented in search of exactly periodic solutions to the 2D, defocusing Majda-McLaughlin-Tabak (MMT) model without forcing or dissipation. We employ two different methods:

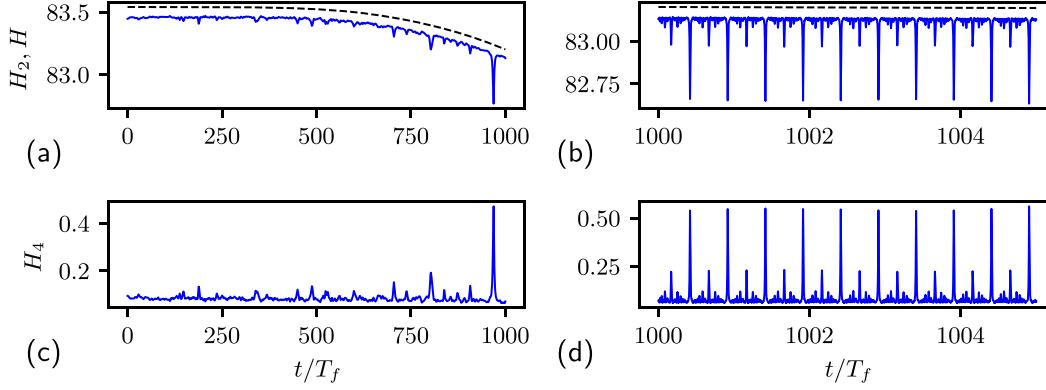


FIG. 13. The time series of (a) H (dashed) and H_2 (solid) starting from $t = 0$ for the defocusing MMT equation with $\beta = 3$ using a scheme that avoids the dealiasing step, with the corresponding time series of (c) H_4 . A detailed view beginning at $t = 1000T_f$ of (b) H , H_2 and (d) H_4 over $5T_f$.

First, we use a traditional method by Flach [30] to obtain breathers in Hamiltonian lattice problems. Second, we use a very recent variational method by Azimi *et al.* [31] for high-degree-of-freedom dynamical systems. Recall that both methods use as an initial condition the numerically obtained quasibreather solution we discuss in the main paper, and our objective is to find a “numerically exact” periodic breather whose state space trajectory is close to the near-periodic one we have observed and reported.

1. Spectral fixed-point method

To implement this method, we require the MMT equation in wave number form, which is given by

$$i \frac{\partial \hat{\psi}_k}{\partial t} = k^2 \hat{\psi}_k + \gamma \sum_{k_1, k_2, k_3} (k_1 k_2 k_3 k)^{\beta/4} \hat{\psi}_{k_1} \hat{\psi}_{k_2} \hat{\psi}_{k_3}^* \delta_K \times (\mathbf{k}_1 + \mathbf{k}_2 - \mathbf{k}_3 - \mathbf{k}). \quad (\text{C1})$$

We introduce the parameter γ to control the size of the nonlinear term, i.e., the nonlinearity level in the main paper. We now assert that $\hat{\psi}_k(t)$ is periodic in time, such that we can write a Fourier series for the solution,

$$\hat{\psi}_k = \sum_n A_{kn} e^{-i\Omega_n t}. \quad (\text{C2})$$

Here we define $\Omega_1 = 2\pi/T$, where T is the prescribed period of the solution. The MMT equation (1) now becomes the system of nonlinear equations,

$$(k^2 - \Omega_n) A_{kn} + \gamma F_{kn} = 0, \quad (\text{C3})$$

where F_{kn} is the full spectral form of the nonlinear term in (1). We now follow the arguments of [30], and we write two fixed-point iteration schemes to find solutions to (C3):

$$A_{kn}^{(i+1)} = \frac{k^2}{\Omega_n} A_{kn}^{(i)} + \frac{\gamma}{\Omega_n} F_{kn}^{(i)}, \quad (\text{C4})$$

$$A_{kn}^{(i+1)} = \frac{\Omega_n}{k^2} A_{kn}^{(i)} - \frac{\gamma}{k^2} F_{kn}^{(i)}. \quad (\text{C5})$$

These schemes share identical fixed points. In the small A_{kn} approximation, the eigenvalues of (C4) and (C5) are given by k^2/Ω_n and Ω_n/k^2 , respectively. These are inverse to one

another, such that if the eigenvalue of one map is greater than 1, the other is less than 1. Thus, for any (\mathbf{k}, n) , we can choose whether or not the mode shrinks or grows in size in the linear approximation. The approach put forth in [30] is to select the fixed-point map for each (\mathbf{k}, n) that ensures that only the fundamental energy-containing mode of the breather grows in the linear approximation. As the A_{kn} evolve under fixed-point iteration, the hope is that a stable fixed point is identified corresponding to a breather with non-negligible amplitude of the energy-containing mode.

We find that the strategy used by Flach to choose the map with an eigenvalue greater than 1 leads to quick divergence of the energy-containing mode in the iteration. Therefore, we apply a modified scheme, where we choose the map with an eigenvalue less than 1 for each mode. With the mapping strategy determined, we can implement the method.

2. Variational method

In this subsection, we adapt the variational method by Azimi *et al.* [31] for finding periodic solutions to nonlinear systems of high dimension. We strongly encourage the reader to first review their article before reading this Appendix. The most important change we make to their derivation is to generalize it for complex scalar fields ψ . Due to nonlocal derivatives, it is better to consider the wave-number form of the MMT equation. We begin by writing the MMT equation in wave-number form (C1). Because this is an evolution equation for the coefficients of a Fourier series, the periodic boundary conditions imposed on our physical domain are automatically satisfied. Thus, the loop space is simply the set of all possible sets of Fourier modes $\{\hat{\psi}_k\}$ that are periodic with a period of T . We can then express a loop I in this loop space as

$$I = \begin{bmatrix} \hat{\psi}_k(t) \\ \hat{\psi}_k^*(t) \\ T \end{bmatrix}, \quad (\text{C6})$$

where $t \in [0, T]$, and \mathbf{k} represents all resolved wave numbers in (1). Note that we have included the conjugate $\hat{\psi}_k^*$ to ensure that gradients with respect to I are well defined for the complex variables $\hat{\psi}_k$ [40]. Just as in [31], we make a substitution of variables such that $t = sT$. Next, we require a suitable inner

product on the loop space. For this, we use the Hermitian inner product

$$\langle I, I' \rangle = \int_0^1 \sum_k (\hat{\psi}_k^* \hat{\psi}'_k + \hat{\psi}_k \hat{\psi}_k^{*'}) ds + TT'. \quad (C7)$$

For this choice of loop space and inner product, the method and conclusions of [31] hold for a periodic complex field subject to nonlocal derivatives as in (1).

We proceed by outlining our derivation of the τ -evolution equation for I . For a given initial loop I_0 , we seek a derivative $\frac{\partial I}{\partial \tau}$ for which the square residual norm $J(I)$ monotonically decreases. The square residual norm is defined by $J(I) \equiv \langle R(I), R(I) \rangle$, where the MMT equation residual is given by

$$R(I) = \begin{bmatrix} R_1 \\ R_2 \\ R_3 \end{bmatrix} \equiv \begin{bmatrix} -\frac{1}{T} \frac{\partial \hat{\psi}_k}{\partial s} - ik^2 \hat{\psi}_k - i \sum_{(k_1, k_2, k_3)} (k_1 k_2 k_3)^{\beta/4} \hat{\psi}_{k_1} \hat{\psi}_{k_2} \hat{\psi}_{k_3}^* \delta_K(\mathbf{k}_1 + \mathbf{k}_2 - \mathbf{k}_3 - \mathbf{k}) \\ \text{c.c.} \\ 0 \end{bmatrix}. \quad (C8)$$

We now assume some $G(I)$ to be the derivative of interest [$\frac{\partial I}{\partial \tau} = G(I)$], and then define

$$\mathcal{L}(I; G) = \lim_{h \rightarrow 0} \frac{R(I + hG) - R(I)}{h} \quad (C9)$$

as the derivative of the residual in the direction of the evolution of I . Reference [31] shows that if $G(I) = -\mathcal{L}^\dagger(I; R)$, where $\mathcal{L}^\dagger(I; R)$ is the adjoint operator to $\mathcal{L}(I; G)$ defined by

$$\langle G, \mathcal{L}^\dagger(I; R) \rangle = \langle \mathcal{L}(I; G), R \rangle, \quad (C10)$$

then $\frac{\partial J}{\partial \tau} \leq 0$ is guaranteed for all τ . It then follows that, for this choice of $G(I)$, any initial guess at a periodic solution to the MMT equation I_0 will evolve in τ until a minimum of J is achieved. If $J \neq 0$, no periodic solution is contained within the basin of attraction. If $J = 0$, a periodic solution has been identified. For our system, the adjoint operator can be found according to (C10) as

$$\mathcal{L}^\dagger(I; R) = \begin{bmatrix} \frac{1}{T} \frac{\partial R_1}{\partial s} + ik^2 R_1 + 2iR_1 k^{-\beta/2} \sum_{k_1} k_1^{-\beta/2} \hat{\psi}_{k_1} \hat{\psi}_{k_1}^* - iR_1^* k^{-\beta/2} \sum_{(k_1, k_2)} (k_1 k_2)^{-\beta/4} \hat{\psi}_{k_1} \hat{\psi}_{k_2} \delta_K(\mathbf{k}_1 + \mathbf{k}_2 - 2\mathbf{k}) \\ \text{c.c.} \\ \frac{2}{T^2} \int_0^1 \sum_k \text{Re} \left[\frac{\partial \hat{\psi}_k^*}{\partial s} R_1 \right] ds. \end{bmatrix}. \quad (C11)$$

With the adjoint operator now determined, we can implement the variational method. For propagation in fictitious time, we use a first-order exponential time differencing scheme to reduce system stiffness.

-
- [1] K. B. Dysthe and K. Trulsen, Note on breather type solutions of the NLS as models for freak-waves, *Phys. Scr.* **T82**, 48 (1999).
- [2] M. Onorato, D. Proment, G. Clauss, and M. Klein, Rogue waves: From nonlinear Schrödinger breather solutions to sea-keeping test, *PLoS ONE* **8**, e54629 (2013).
- [3] J. M. Dudley, F. Dias, M. Erkintalo, and G. Genty, Instabilities, breathers and rogue waves in optics, *Nat. Photon.* **8**, 755 (2014).
- [4] C.-C. Ding, Y.-T. Gao, and L.-Q. Li, Breathers and rogue waves on the periodic background for the Gerdjikov-Ivanov equation for the Alfvén waves in an astrophysical plasma, *Chaos, Solitons & Fractals* **120**, 259 (2019).
- [5] *The Sine-Gordon Model and Its Applications*, edited by J. Cuevas-Maraver, P. G. Kevrekidis, and F. Williams, Nonlinear Systems and Complexity Vol. 10 (Springer International, Cham, 2014).
- [6] M. Tajiri and Y. Watanabe, Breather solutions to the focusing nonlinear Schrödinger equation, *Phys. Rev. E* **57**, 3510 (1998).
- [7] S. Clarke, R. Grimshaw, P. Miller, E. Pelinovsky, and T. Talipova, On the generation of solitons and breathers in the modified Korteweg–de Vries equation, *Chaos* **10**, 383 (2000).
- [8] K. W. Chow, R. H. J. Grimshaw, and E. Ding, Interactions of breathers and solitons in the extended Korteweg–de Vries equation, *Wave Motion* **43**, 158 (2005).
- [9] S. Flach and A. V. Gorbach, Discrete breathers – Advances in theory and applications, *Phys. Rep.* **467**, 1 (2008).
- [10] E. Trías, J. J. Mazo, and T. P. Orlando, Discrete breathers in nonlinear lattices: Experimental detection in a josephson array, *Phys. Rev. Lett.* **84**, 741 (2000).
- [11] A. E. Miroshnichenko, S. Flach, M. V. Fistul, Y. Zolotaryuk, and J. B. Page, Breathers in Josephson junction ladders: Resonances and electromagnetic wave spectroscopy, *Phys. Rev. E* **64**, 066601 (2001).
- [12] R. Livi, M. Spicci, and R. S. MacKay, Breathers on a diatomic FPU chain, *Nonlinearity* **10**, 1421 (1997).
- [13] T. Cretegny, T. Dauxois, S. Ruffo, and A. Torcini, Localization and equipartition of energy in the beta-FPU chain: Chaotic breathers, *Physica D* **121**, 109 (1998).
- [14] B. Rumpf and A. C. Newell, Coherent structures and entropy in constrained, modulationally unstable, nonintegrable systems, *Phys. Rev. Lett.* **87**, 054102 (2001).
- [15] B. Rumpf, Simple statistical explanation for the localization of energy in nonlinear lattices with two conserved quantities, *Phys. Rev. E* **69**, 016618 (2004).
- [16] G. Fodor, P. Forgács, P. Grandclément, and I. Rácz, Oscillons and quasibreathers in the ϕ^4 Klein-Gordon model, *Phys. Rev. D* **74**, 124003 (2006).

- [17] A. M. Eremin, P. V. Zakharov, M. D. Starostenkov, and A. S. Vdovin, Analysis of statistical characteristics of quasi-breather in monatomic fcc metals Au, Cu, Ni, Pd and Pt, *Condens. Matter Interphases* **20**, 596 (2018).
- [18] A. Pushkarev and V. E. Zakharov, Quasibreathers in the MMT model, *Physica D* **248**, 55 (2013).
- [19] V. E. Zakharov, P. Guyenne, A. N. Pushkarev, and F. Dias, Wave turbulence in one-dimensional models, *Physica D* **152-153**, 573 (2001).
- [20] B. Rumpf, A. C. Newell, and V. E. Zakharov, Turbulent transfer of energy by radiating pulses, *Phys. Rev. Lett.* **103**, 074502 (2009).
- [21] B. Rumpf and A. C. Newell, Wave instability under short-wave amplitude modulations, *Phys. Lett. A* **377**, 1260 (2013).
- [22] B. Rumpf and T. Y. Sheffield, Transition of weak wave turbulence to wave turbulence with intermittent collapses, *Phys. Rev. E* **92**, 022927 (2015).
- [23] R. Saint-Jalm, P. C. M. Castilho, E. Le Cerf, B. Bakkali-Hassani, J.-L. Ville, S. Nascimbene, J. Beugnon, and J. Dalibard, Dynamical symmetry and breathers in a two-dimensional Bose gas, *Phys. Rev. X* **9**, 021035 (2019).
- [24] H. S. Dumas, *The KAM Story: A Friendly Introduction to the Content, History, and Significance of Classical Kolmogorov–Arnold–Moser Theory* (World Scientific, Singapore, 2014).
- [25] S. Nazarenko, *Wave Turbulence*, Lecture Notes in Physics Vol. 825 (Springer, Berlin, 2011).
- [26] A. J. Majda, D. W. McLaughlin, and E. G. Tabak, A one-dimensional model for dispersive wave turbulence, *J. Nonlin. Sci.* **7**, 9 (1997).
- [27] A. Hrabski and Y. Pan, Effect of discrete resonant manifold structure on discrete wave turbulence, *Phys. Rev. E* **102**, 041101(R) (2020).
- [28] A. Hrabski and Y. Pan, On the properties of energy flux in wave turbulence, *J. Fluid Mech.* **936**, A47 (2022).
- [29] See Supplemental Material at <http://link.aps.org/supplemental/10.1103/PhysRevE.108.054215> for an animation of the quasi-breather.
- [30] S. Flach, Obtaining breathers in nonlinear Hamiltonian lattices, *Phys. Rev. E* **51**, 3579 (1995).
- [31] S. Azimi, O. Ashtari, and T. M. Schneider, Constructing periodic orbits of high-dimensional chaotic systems by an adjoint-based variational method, *Phys. Rev. E* **105**, 014217 (2022).
- [32] J. Bourgain, Quasi-periodic solutions of hamiltonian perturbations of 2D linear schrödinger equations, *Ann. Math.* **148**, 363 (1998).
- [33] J. Geng, X. Xu, and J. You, An infinite dimensional KAM theorem and its application to the two dimensional cubic Schrödinger equation, *Adv. Math.* **226**, 5361 (2011).
- [34] C. Procesi and M. Procesi, A KAM algorithm for the resonant non-linear Schrödinger equation, *Adv. Math.* **272**, 399 (2015).
- [35] X. Yuan, Construction of quasi-periodic breathers via KAM technique, *Commun. Math. Phys.* **226**, 61 (2002).
- [36] D. Bambusi and D. Vella, Quasi periodic breathers in Hamiltonian lattices with symmetries, *Discrete Contin. Dyn. Syst. B* **2**, 389 (2002).
- [37] J. Geng, J. Viveros, and Y. Yi, Quasi-periodic breathers in Hamiltonian networks of long-range coupling, *Physica D* **237**, 2866 (2008).
- [38] Y.-C. Lai, D.-R. He, and Y.-M. Jiang, Basins of attraction in piecewise smooth Hamiltonian systems, *Phys. Rev. E* **72**, 025201(R) (2005).
- [39] J. M. Sanz-Serna and M. P. Calvo, *Numerical Hamiltonian Problems*, illustrated ed. (Dover, Mineola, NY, 2018).
- [40] K. Kreutz-Delgado, The complex gradient operator and the CR-calculus, *Phys. Rev. E* (to be published), [arXiv:0906.4835](https://arxiv.org/abs/0906.4835).